Clay Nanosheets in Skeletons of Controlled Phase Inversion Separators for Thermally Stable Li-Ion Batteries

*Min Kim, Jung Kyu Kim, and Jong Hyeok Park**

Phase inversion is a powerful alternative process for preparing ultra-thin separators for various secondary batteries. Unfortunately, separators prepared from phase inversion generally suffer from uneven pore size and pore size distribution, which frequently results in poor battery performance. Here, a straightforward route is demonstrated to solve the drawbacks of phase-inversion-based separators for Li-ion batteries by means of directly incorporating 2D clay sheets in the skeleton of poly(vinylidene fluoride-*co*-hexafluoropropylene) (PVdF-HFP) with multiscale pore generation from a simple one-step solution coating method. Additionally generated pores by the inclusion of 2D nanosheets in PVdF-HFP skeletons, combined with the multiscale pores (several micrometers + sub-micrometers) originally generated by means of the controlled phase inversion, can generate additional ionic transport pathways, leading to Li-ion battery performances better than those of commercialized polyethylene separators. Moreover, the addition of extremely low contents of 2D clay sheets in PVdF-HFP separators allows thermally stable polymer separators to be realized.

1. Introduction

Li-ion battery components, including the cathode, anode, electrolyte, and separator, are under development to fulfill standard requirements of electric or hybrid-electric vehicles (EVs or HEVs).[1–7] Even though many kinds of emerging cathode and anode materials with high specific capacities have been reported recently, the separators in commercialized Li-ion batteries are still being made of polyethylene (PE) or polypropylene because of these materials' uniform pore size, high tensile strength, and chemical stability.[8–10] However, these materials also have poor thermal and dimensional stability, which has raised serious concerns over the ability to maintain safety in Li-ion batteries under abnormal heating or hard internal shorting, and cell performance also should be improved for next-generation Li-ion batteries. Recently, the phase inversion method has received attention as an effective way to prepare porous membranes, which are based on poly(vinylidene fluoride-*co*-hexafluoropropylene) (PVdF-HFP) polymer dissolved in a controlled mixture of a good solvent and a poor solvent.[11–13] Even though reasonable pores have been obtained in PVdF-HFP membranes using the phase inversion method, finer control over the pore size and size distribution of the separators are still challenging issues in order to realize cell performance exceeding that of cells using conventional PE separators.[11–20]

In our previous report, a novel facial approach was adopted to provide multiscale pore structure in a PVdF-HFP membrane by means of a controlled phase inversion method, including a more finely controlled evaporation rate of the good solvent and the poor solvent.[21] By combining two different PVdF-HFP polymers having different phase inversion behaviors, we introduced a new paradigm for the preparation of separators of Li-ion batteries that can meet standard application requirements for battery separators, such as charge/discharge performance, cycle performance, and dimensional stability.

In the present work, exfoliated clay 2D nanosheets were simply dispersed into PVdF-HFP skeletons, which originally had multiscale pore structures (**Figure 1**A). First, additional pores generated from exfoliated 2D nanosheets in PVdF-HFP skeletons combined with the original multiscale pores generated by controlled phase inversion can generate additional ionic transport pathways, thereby improving separator performance. Second, PVdF-HFP-incorporating 2D nanosheets exhibited greatly improved thermal stability that decreased the possibility of battery short circuit, thereby enhancing battery safety.

2. Results and Discussion

The use of two different acetone evaporation rates during the drying process leads to two different phase separation paths that produce two different PVdF-HFP polymers (Figure 1B). In this study, 18-μm-thick wet-laid nonwoven (Figure S1, Supporting Information) was used as the mother substrate for the PVdF-HFP-based separator, and the PVdF-HFP polymer solution with well-dispersed clay nanoparticle was coated onto the nonwoven substrate by a dip-coating method, followed by drying at 25 °C and 40% relative humidity. Because clay nanoparticles are

M. Kim, J. K. Kim
School of Chemical Engineering
Sungkyunkwan University
Suwon 440-746, Republic of Korea
Prof. J. H. Park
Department of Chemical and Biomolecular Engineering
Yonsei University
50 Yonsei-ro, Seodaemun-gu
Seoul 120-749, Republic of Korea
E-mail: lutts@skku.edu

DOI: 10.1002/adfm.201500758

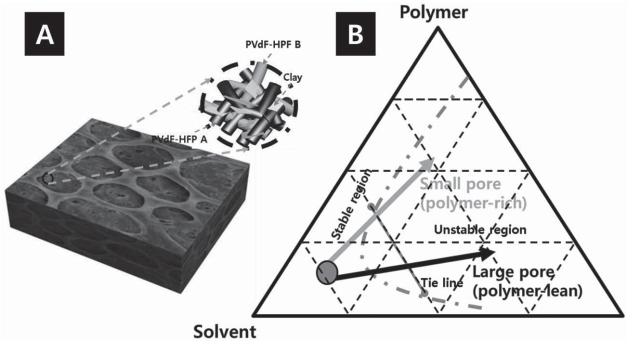

Figure 1. a) Schematic diagram of the proposed nanocomposite separator of PVdF-HFP and 2D clay nanosheets prepared by b) controlled phase inversion; pore structure resulting from fast phase inversion (black, PVdF-HFP A (12 wt% HFP)) and pore structure resulting from slow phase inversion (gray, PVdF-HFP, B (6 wt% HFP)).

strongly hydrophilic, the particles were dispersed in nonsolvent phase (water) (Figure S2, Supporting Information), followed by mixing with PVdF-HFP/acetone solution (see the Experimental Section for more details).

First, the effectiveness of adding clay nanoparticles upon the generation of pores in PVdF-HFP was investigated. The fabricated PVdF-HFP films had both large (~several micrometers) and small pores (~sub-micrometers), but the addition of clay nanoparticles to the film seemed not to greatly influence its macroscopic morphology (**Figure 2**). Well-dispersed and nanosized clay nanoparticles were not visible in scanning electron microscope (SEM) observation. To confirm the existence of clay nanoparticles in the PVdF-HFP skeleton, small-angle X-ray scattering (SAXS) patterns of the PVdF-HFP films with and without clay nanoparticles were investigated (**Figure 3**A). In general, the crystallization of semicrystalline polymers may be disturbed by the addition of inorganic nanoparticles.[19,22–37] Our SAXS data also provided evidence for this morphology transition of the film because of the clay nanoparticles. The original SAXS peak of the PVDF-HFP film around $q = 1$ was weakened and almost disappeared in samples to which clay nanoparticles has been added, indicating that the domain structure of the blends became disordered.

In general, thermogravimetric analysis (TGA) of polymer nanocomposites containing clay nanoparticles showed that the thermal stability of the polymer was improved (as indicated by a higher onset temperature of degradation) when clay nanoparticles were incorporated into the polymer matrix. The outcome of the clay nanoparticle layered structure has been more explained as exceptional insulation and mass transport barrier against the capricious compounds generated during the decomposition of polymer under thermal conditions.[22–24] In a TGA analysis of PE separator, PVdF-HFP separator, and clay nanocomposite PVdF-HFP separator materials (Figure 3B), the conventional PE materials began to lose mass sharply at 450 °C, and nearly 100% of their mass was lost by 490 °C, even in a nitrogen environment. In stark contrast, the PVdF-HFP polymer started to lose mass at a similar temperature, but retained more than 50% of its mass even up to 500 °C, and the mass retention was not improved much for PVdF-HFP/clay composites. Even though all the PVdF-HFP separators tested had excellent dimensional stability (Figure S3, Supporting Information), the stability of the porous structure was strongly influenced by the presence of clay in the film (**Figure 4**). Initially, the pure PVdF-HFP separator and PVdF-HFP/clay separator had nearly identical pore structures. However, when these two types of separators were thermally treated at 150 °C and 200 °C, respectively, for 30 min, it was observed that the PVdF-HFP/clay separators retained their original pore shapes even at 200 °C, whereas the pure PVdF-HFP separators melted down and lost their porous structure, which also confirm the improved thermal and dimensional stability of the PVdF-HFP separator with added clay.

One of the important requirements for a separator in a Li-ion battery is its ability to transport ions between the anode and cathode. As the clay loading level was increased, the ionic conductivity of the resulting PVdF-HFP separator also increased (**Figure 5**A). Thus, the addition of a small amount of clay in the deionized (DI) water to the PVdF-HFP substrate is potentially beneficial not only for preserving the original multiscale pore distribution of PVdF-HFP film, but also for increasing the ionic conductivity. It is well known that the presence and mobility of ions present in the clay structure can determine the ionic conductivity.[22–34] As expected, 0.004 wt% of clay increased the ionic conductivity (σ) from 1.15×10^{-3} to 1.19×10^{-3} S cm^{-1}. When 0.008 wt% of clay was added, σ increased to 1.27×10^{-3} S cm^{-1}; further increases in clay content continued to increase σ until in plateaued at the clay content of 0.028 wt%. The maximum ionic conductivity of 1.49×10^{-3} S cm^{-1} was obtained for the added clay content of 0.04 wt%, due to the increase of the interfacial area between clay layers and polymer chains, through which the lithium ion can move more easily. In Figure 5B, the porosity of the PVdF-HFP/clay nanocomposite separators, ϕ_p(%), was estimated using the following equation, in which W_c is the weight per square meter of the PVdF-HFP/clay coating layer, W_N is the weight per square meter of the

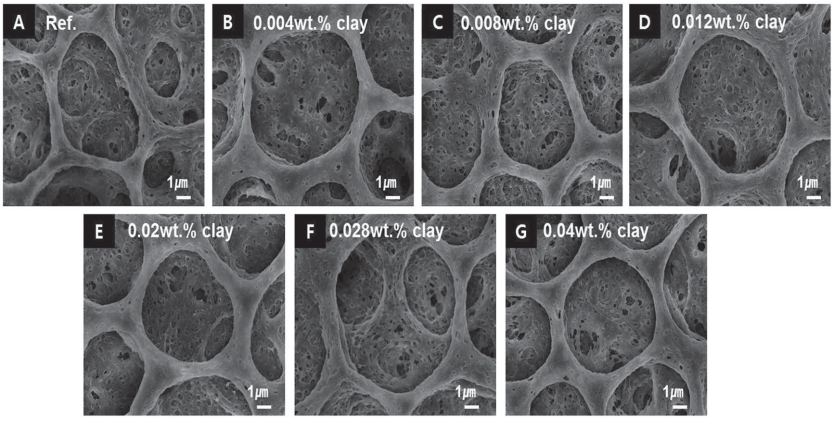

Figure 2. SEM images of the surfaces of PVdF-HFP separators prepared using a 7:3 ratio of PVdF A to B, by weight, with various clay nanosheet contents: A) 0 wt%, B) 0.004 wt%, C) 0.008 wt%, D) 0.0012 wt%, E) 0.02 wt%, F) 0.028 wt%, G) 0.04 wt%.

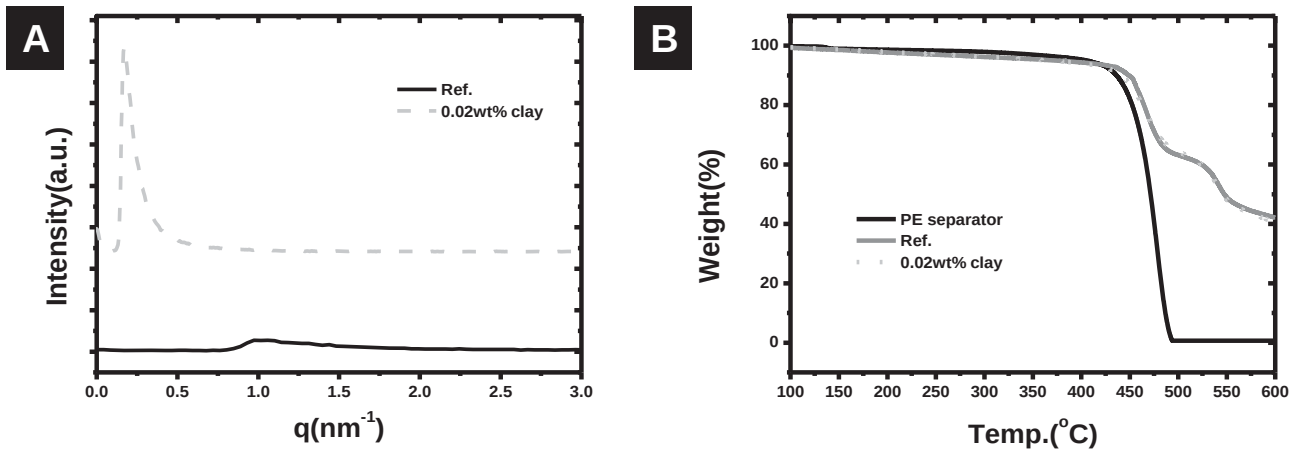

Figure 3. A) SAXS data; Ref = PVdF A/PVdF B=7/3 by weight, B) Thermogravimetric curves of the PVdF-HFP/clay nanocomposite separator.

nonwoven, ρ_c is the density of the PVdF-HFP/clay coating layer, ρ_N is the density of the nonwoven, and V_{NC} is the volume of the PVdF-HFP/clay.[38]

$$\phi_p(\%) = \{1 - [(W_c/\rho_c + W_N/\rho_N)/V_{NC}]\} \times 100$$

The porosity of a Li-ion battery separator indicates how easily Li-ions can move back and forth between the anode and cathode. More porous separators allow freer ion pathways with less internal resistance. In general, Li-ion battery separators have porosity of 35%–50%.[8–10] The porosity of the PVdF-HFP/clay nanocomposite separators was not greatly influenced by changing the clay loading level, although a slight increase in porosity was noticed as the clay content was increased (Figure 5B). In addition, we investigated the formation of additional pores in the PVdF-HFP separator after adding the clay nanoparticles. For this experiment, we used mercury porosimetry technique. As shown in Figure S4 (Supporting Information), more increased population of small pores in the PVdF-HFP/clay nanocomposite separator was observed, which might be originated from the interfaces of PVdF-HFP and clay nanosheets. Especially, the population of pore sizes between 50 nm and 2 μm was notably increased. From this result, we can confirm that the inclusion of 2D nanosheets in PVdF-HFP skeletons can provide additional pathways for Li- ion transport.

The electrochemical stability window of the PVdF-HFP/clay separators was monitored using linear sweep voltammetry (LSV). For the LSV measurements, coin-type cells were prepared in which the PE or PVdF-HFP/clay separators were sandwiched between Li foil and a stainless steel plate. For all systems considered, the current onsets were detected over 7.0 V versus Li, which can be assigned to the stable window of the separators. The LSV data indicated that various samples show almost identical oxidative behaviors (**Figure 6**A), verifying that the addition of small amounts of exfoliated clay in the DI water to the PVdF-HFP matrix does not negatively affect the intrinsic electrochemical properties of the PVdF-HFP separator. For practical application of the prepared separators, galvanostatic

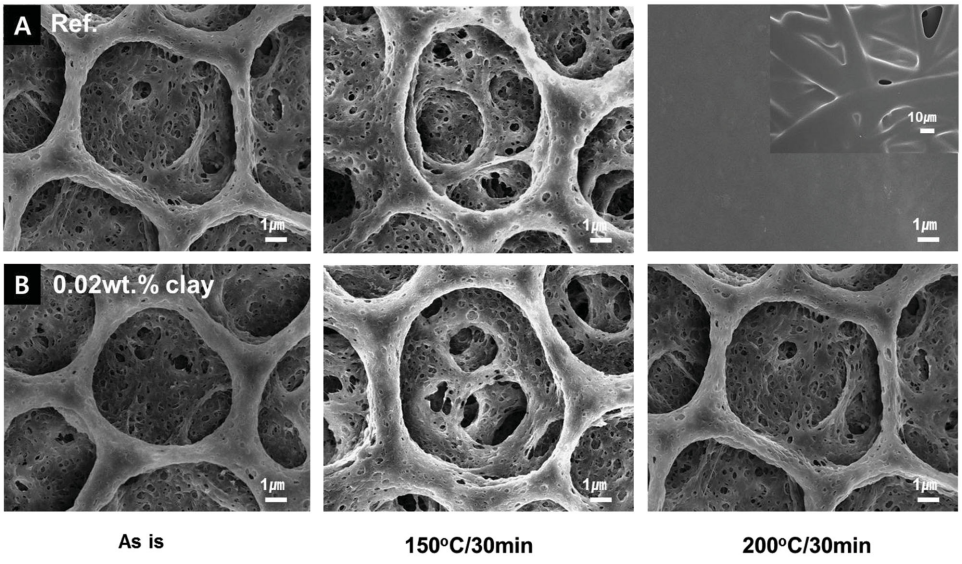

Figure 4. SEM images of the PVdF-HFP/clay nanocomposite separator before and after being stored at 150 °C/200 °C for 30 min.

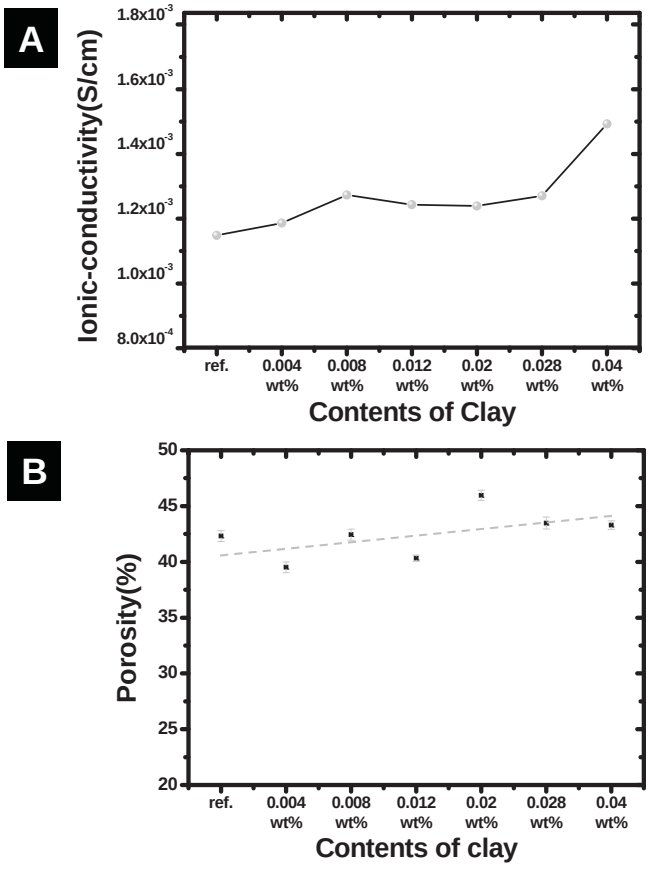

Figure 5. A) Ionic conductivity at 25 °C and B) porosity of composite separators with various contents of exfoliated clay.

charge/discharge tests of full cells ($LiCoO_2$/separator/MCMB) were performed. First, the open-circuit voltage (OCV) drop behavior of a cell is directly related to the self-discharge (Figure 6B). This information can be used to predict the risk of an internal short circuit occurring between the cathode and anode, which could lead to a fire or an explosion of the cell. The cell assembled with the PVdF-HFP/clay separator exhibited an appreciably small OCV drop compared to that of the neat PVdF-HFP separator and the PE separator (Figure 6B). In addition, we observed voltage profiles of charged coin cells in the hot box, which maintains constant temperature of 150 °C. As shown in Figure S5 (Supporting Information), we could see the positive effects of clay nanosheets for the thermal stability, in which the inclusion of 2D nanosheets in PVdF-HFP skeletons can block internal short circuit occurring between the cathode and anode. Second, the rate capability was evaluated by charging a cell at a constant current of 0.2 C and then discharging it by increasing the current rate from 0.2 C to 3 C. A linear capacity drop was observed with increasing C-rate for all of the cells (Figure 6C). This behavior was influenced by the electrical polarization caused by the increase in the serial resistance as the discharge C-rate was increased. The discharge capacities of the modified PVdF-HFP separators with optimum clay content showed superior performance to that of the pure PVdF-HFP separator. The overall performance was optimized by using the exfoliated clay content of 0.04 wt%.

The effect upon the cycling performance of using higher exfoliated clay contents was further electrochemically examined using the 0.5 C rate of charge and discharge. Figure 6D compares the cyclability of the modified PVdF-HFP separators with those of the PE separator and neat PVdF-HFP separators, which were characterized by the discharge capacity as a function of the cycle number. The coin cells were cycled between 3 and 4.3 V at a constant charge/discharge current density (0.5 C/0.5 C). Obviously, the PVdF-HFP/clay composite separators exhibited much improved discharge capacity retention after 100 cycles than the PE separators and neat PVdF-HFP separators. An intriguing finding in Figure 6D is that the formation of additional pores due to inclusion of 2D nanosheets in PVdF-HFP skeletons could improve discharge capacity retention after 100 cycles, which is greater than those of the pristine PE separator and the original PVdF-HFP separators. In PVdF-HFP separators with clay nanoparticles, the additional ionic paths and increased electrolyte uptake from the increased porosity might be the origin of greatly improved cyclic performances.

3. Conclusion

Inclusion of clay nanosheets in skeletons of PVdF-HFP could generate additional pores for improved electrochemical properties and thermal stability of Li-ion battery separators. Because the separators were prepared by a simple one-step phase inversion method, the proposed process is extremely cost-effective way. This method triggered a finely controlled phase inversion, producing additional ionic transport pathways by means of the direct dispersion of 2D clay sheets within the PVdF-HFP skeleton with original multiscale pores in the PVdF-HFP itself. The use of these separators to replace commercial PE represented greatly improved C-rate and cyclic performances of Li-ion batteries as well as high thermal stabilities. Therefore, the proposed separator is a promising alternative to PE separators for future energy-storage applications.

4. Experimental Section

Preparation of the PVdF-HFP Separator with Exfoliated 2D Clay Nanosheets: By following a previously reported procedure, multiscale pores were generated in PVdF-HFP separators by using two kinds of PVdF-HFP with different HFP contents (12 wt% for "PVdF A" and 6 wt% for "PVdF B").[21] To prepare well-exfoliated 2D clay nanosheet solution, the clay powders (Na-MMT clay, Cloisite R+) was dispersed in DI water adjusted to have pH 7.3 and the suspended solution was stirred at 1000 rpm for 30 min. The suspended solution was ultrasonicated for 1 h by using a ULH 700S Sonosmasher (Ulsso Hightech, Korea) to achieve complete dispersion and exfoliation; the resulting clay solution was transparent (Figure S2, Supporting Information). Then, PVdF-HFP/acetone solution and clay/water solution were mixed to have 4 wt% water in the resulting acetone/water solvent mixture (i.e., 4% water/(water + acetone) by mass). A wet-laid nonwoven coating substrate around 18 μm thick was used for a solution dip-coating process. Note that the nonwoven itself had large pores of several hundred micrometers (Figure S1, Supporting Information), making it impossible to be used directly for separators of Li-ion batteries. The PVdF-HFP/clay solutions were coated onto the nonwoven by dip-coating, followed by drying at 25 °C and 40% relative humidity. The clay contents in the PVdF-HFP/clay composite separators were controlled between 0.004 and 0.04 wt%.

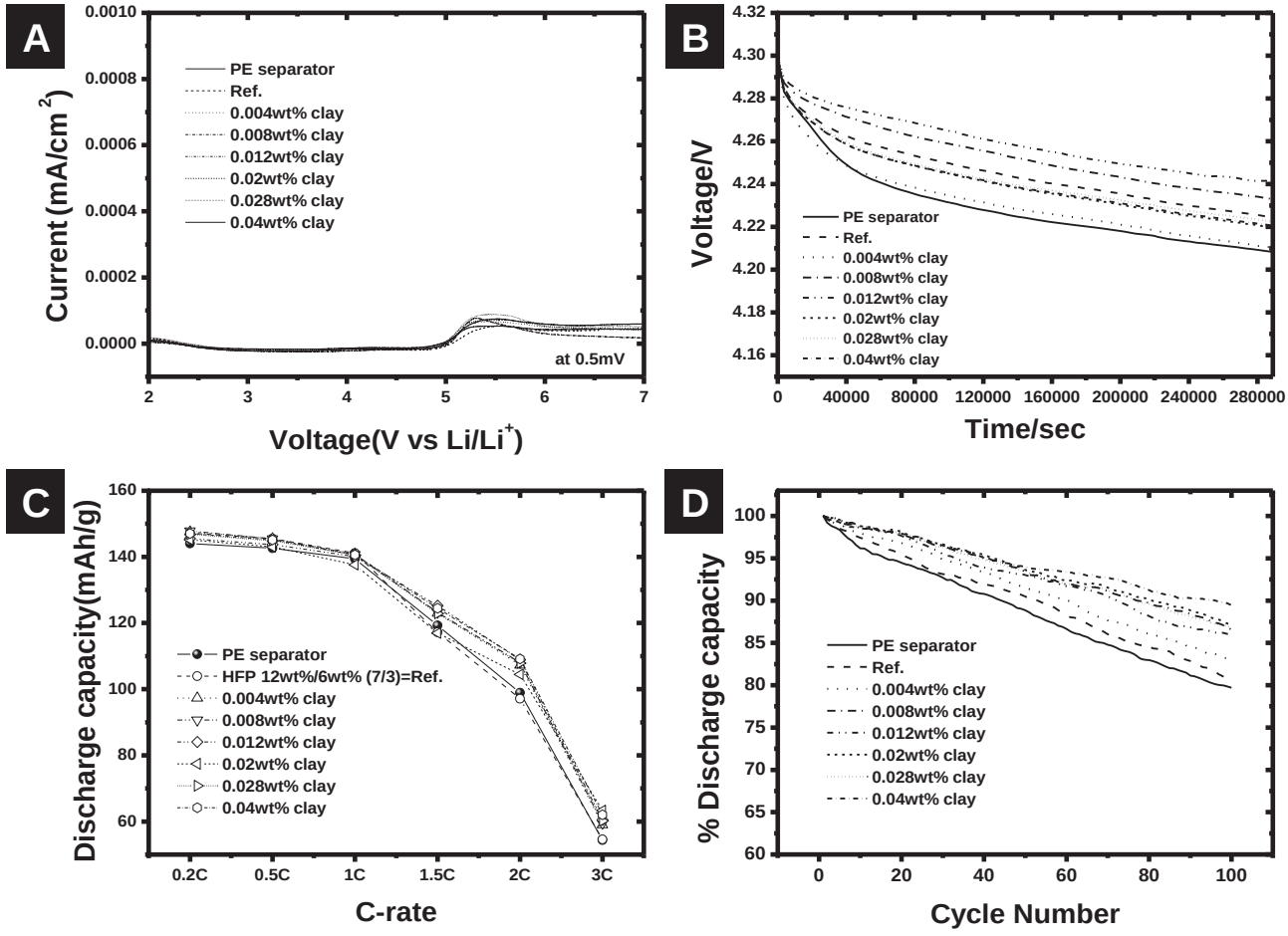

Figure 6. Performance of composite separators with various contents of exfoliated clay: A) LSV curves, B) OCV decay curves, C) discharge capacities of the unit cell at various discharge rates after charging at 0.2 C, D) cycle performance.

Characterization of Physicochemical Properties and Electrochemical Performance of the PVdF-HFP Separator Incorporating Exfoliated 2D Clay Nanosheets: The morphology of the PVdF-HFP/clay separator was examined by using a field-emission scanning electron microscope (FE-SEM, JSM-7000). Evidence of and information on the exfoliated 2D clay sheets was obtained by means of SAXS analysis. SAXS is a technique that has been particularly suitable for elucidating the nanomorphology adopted by the microphase separation typical of the PVdF-HFP/clay complex materials, including particle size and size distribution, particle shape (sphere, cylinder, lamella), and internal structure (core–shell), porosity (surface-to-volume ratio), order (crystallinity), and orientation of the particles. SAXS analysis was carried out by using a SAXSess camera (Anton-Paar, Graz, Austria) and an X-ray generator (Philips, PW 1730/10) operated at 40 kV and 50 mA with a sealed-tube Cu anode. A Göbel mirror was used to convert the divergent polychromatic X-ray beam into a collimated line-shaped beam of Cu Kα radiation ($\lambda = 0.154$ nm). The 2D scattering pattern was recorded by an imaging-plate detector (model Fuji BAS1800 from Raytest, Straubenhardt, Germany) and integrated into the 1D scattering function $I(q)$ by using SAXSQuant software (Anton-Paar). The scattering vectors q attained by this configuration ranged from 0.01 to 3 nm^{-1}. The PVdF-HPF/clay samples were pressed into a 1 mm slit within an Al plate and mounted directly in the camera without using any additional window for the sample holder (5 × 20 mm) and measured at 25 °C. The sample-to-detector distance of 25 cm was used. To examine the thermal transition behavior of the modified separator, the samples were observed after the separator was placed in an oven and heated at 150–200 °C for 30 min. Thermogravimetric analysis (TGA 6000, Seiko Instruments) was then used to evaluate the thermal properties of the modified separators. The modified separators were heated from 25 °C to 600 °C at the rate of 10 °C min^{-1} under N_2 atmosphere. The ionic conductivity (σ) of the separator was determined by AC impedance spectroscopy (IM6-6eX) within the frequency range of 0.01–100 kHz. An AC perturbation of 5 mV was applied to the cell. LSV was performed to investigate the electrochemical window of the separator by using a coin-type cell in which a stainless steel served as the working electrode and lithium served as both counter and reference electrodes. The LSV was carried out by using an electrochemical workstation (CHI-660, CH Instruments) system, using the scan rate of 1 mV s^{-1} over the range of 0 to 7.0 V (versus Li/Li^+). The OCV drop behavior was investigated, which is directly related to the self-discharge. For this characterization, unit cells were charged to 4.3 V and their voltage drop was continuously monitored as a function of elapsed time at room temperature. For evaluation of cell performance, a unit cell was assembled. The composition of the anode was 94 wt% graphitized mesocarbon microbeads (MCMB2528) and 6 wt% Kynar 741 as a polymeric binder. The cathode was composed of 90 wt% $LiCoO_2$, 6 wt% Super-P, and 4 wt% PVdF. The electrolyte used for the coin cell (2032 type) was $LiPF_6$ (1 M) with EC/DEC/EMC (1:1:1, v/v/v). The lithium coin cell was assembled by sandwiching the surface-modified separator between an MCMB anode and a $LiCoO_2$ cathode, and then activated by filling the space between them with the liquid electrolyte. For the charge/discharge test, the cells were charged up to 4.3 V at the rate of 0.2 C and then discharged to 3.0 V at various C-rates. The charge process was cut off at 20% of the initial constant current. The cells were cycled at a fixed charge/discharge current density of 0.5 C/0.5 C.

Supporting Information

Supporting Information is available from the Wiley Online Library or from the author.

Acknowledgements

This work was supported by the NRF of KoreaGrant funded by the Ministry of Science, ICT & Future Planning (2009-0083540, NRF-2013R1A2A1A09014038).

Received: February 25, 2015
Published online: April 17, 2015

[1] B. Scrosati, J. Hassoun, Y. K. Sun, *Energy Environ. Sci.* **2011**, *4*, 3287.
[2] B. Scrosati, *Nat. Nanotechnol.* **2007**, *2*, 598.
[3] Y. G. Guo, J. S. Hu, L. J. Wan, *Adv. Mater.* **2008**, *20*, 2878.
[4] T. H. Kim, J. S. Park, S. K. Chang, S. C. Choi, J. H. Ryu, H. K. Song, *Adv. Energy Mater.* **2012**, *2*, 860.
[5] H. Nishide, K. Oyaizu, *Science* **2008**, *319*, 737.
[6] B. Kang, G. Ceder, *Nature* **2009**, *458*, 190.
[7] J. M. Tarascon, M. Armad, *Nature* **2001**, *414*, 359.
[8] S. S. Zhang, *J. Power Source* **2007**, *164*, 351.
[9] P. Arora, Z. Zang, *Chem. Rev.* **2004**, *104*, 4419.
[10] J. R. Kim, S. W. Choi, S. M. Jo, W. S. Lee, B. C. Kim, *J. Electrochem. Soc.* **2005**, *152*, A295.
[11] Z. Cui, E. Drioli, Y. M. Lee, *Prog. Polym. Sci.* **2014**, *39*, 164.
[12] W. Pu, X. He, L. Wang, C. Jiang, C. Wan, *J. Membr. Sci.* **2006**, *272*, 11.
[13] A. M. Stephan, Y. Saito, *Solid State Ionics* **2002**, *148*, 475.
[14] F. Boudin, X. Andrieu, C. Jehoulet, *J. Power Source* **1999**, *81*, 804.
[15] Z. H. Li, G. Y. Su, X. Y. Wang, *Solid State Ionics* **2005**, *176*, 23.
[16] F. Corce, M. L. Focarete, J. Hassoun, I. Meschini, B. Scrosati, *Energy Environ. Sci.* **2011**, *4*, 921.
[17] X. Cao, J. Ma, X. Shi, Z. Ren, *Appl. Surf. Sci.* **2006**, *253*, 2003.
[18] Z. H. Li, G. Y. Su, X. Y. Wang, *Solid State Ionics* **2005**, *176*, 23.
[19] S. Srivastava, J. L. Schaefer, Z. Yang, Z. Tu, L. A. Acrher, *Adv. Mater.* **2014**, *26*, 201.
[20] P. P. Prosini, P. Villano, M. Carewska, *Electrochem. Acta* **2002**, *48*, 227.
[21] M. Kim, J. H. Park, *Adv. Energy Mater.* **2013**, *3*, 1417.
[22] Y. Kojima, A. Usuki, M. Kawasumi, A. Okada, Y. Fukushima, T. Kurauchi, O. Kamigaito, *J. Mater. Res.* **1993**, *8*, 1185.
[23] Y. Kojima, A. Usuki, M. Kawasumi, A. Okada, Y. Fukushima, T. Kurauchi, O. Kamigaito, *J. Appl. Polym. Sci.* **1993**, *49*, 1259.
[24] P. C. Lebaron, Z. Wang, T. J. Pinnavaia, *Appl. Clay Sci.* **1999**, *15*, 11.
[25] K. K. Bissada, W. D. Johns, F. S. Cheng, *Clay Minerals* **1967**, *7*, 155.
[26] M. J. Koh, H. Y. Hwang, D. J. Kim, H. J. Kim, Y. T. Hong, S. Y. Nam, *J. Mater. Sci. Technol.* **2010**, *26*, 633.
[27] B. Reddy, *Advances in Diverse Industrial Applications of Nanocomposites*, InTech, Rijeka, Croatia **2014**, p.113.
[28] L. Priya, J. P. Jog, *J. Polym. Sci., Part B: Polym. Phys.* **2003**, *41*, 31.
[29] K. P. Pramoda, A. Mohamed, I. Y. Phang, T. Liu, *Polym. Int.* **2005**, *54*, 226.
[30] E. P. Giannelis, *Adv. Mater.* **1996**, *8*, 29.
[31] J. Wang, Z. Y. Liu, C. Y. Guo, Y. J. Chen, D. Wang, *Macromol. Rapid Commun.* **2001**, *22*, 1422.
[32] K. Yano, A. Usuki, A. Okada, T. Kurauchi, O. Kamigaito, *J. Polym. Sci., Part A: Polym. Chem.* **1993**, *31*, 2493.
[33] D. R. Paul, L. M. Robeson, *Polymer* **2008**, *49*, 3187.
[34] J. W. Gilman, *Appl. Clay Sci.* **1999**, *15*, 31.
[35] K. Norrish, *Discuss. Faraday Soc.* **1954**, *18*, 120.
[36] M. Morvan, D. Espinat, J. Lambard, Th. Zemb, *Colloids Surf. A: Physicochem. Eng. Aspects* **1994**, *82*, 193.
[37] T. Rieker, A Hanprasopwattana, A. Datye, P. Hubbard, *Langmuir* **1999**, *15*, 638.
[38] E. S. Choi, S. Y. Lee, *J. Mater. Chem.* **2011**, *21*, 14747.